

July 2002

In-plane elastic stability of arches under a centra concentrated load

M. A. Bradford
University of New South Wales

B. Uy
University of New South Wales, brianuy@uow.edu.au

Y. L. Pi
University of New South Wales

Follow this and additional works at: <https://ro.uow.edu.au/engpapers>



Part of the [Engineering Commons](#)

<https://ro.uow.edu.au/engpapers/209>

Recommended Citation

Bradford, M. A.; Uy, B.; and Pi, Y. L.: In-plane elastic stability of arches under a centra concentrated load 2002.
<https://ro.uow.edu.au/engpapers/209>

In-Plane Elastic Stability of Arches under a Central Concentrated Load

M. A. Bradford, M.ASCE¹; B. Uy, M.ASCE²; and Y.-L. Pi³

Abstract: This paper is concerned with the in-plane elastic stability of arches with a symmetric cross section and subjected to a central concentrated load. The classical methods of predicting elastic buckling loads consider bifurcation from a prebuckling equilibrium path to an orthogonal buckling path. The prebuckling equilibrium path of an arch involves both axial and transverse deformations and so the arch is subjected to both axial compression and bending in the prebuckling stage. In addition, the prebuckling behavior of an arch may become nonlinear. The bending and nonlinearity are not considered in prebuckling analysis of classical methods. A virtual work formulation is used to establish both the nonlinear equilibrium conditions and the buckling equilibrium equations for shallow arches. Analytical solutions for antisymmetric bifurcation buckling and symmetric snap-through buckling loads of shallow arches subjected to this loading regime are obtained. Approximations for the symmetric buckling load of shallow arches and nonshallow fixed arches and for the antisymmetric buckling load of nonshallow pin-ended arches, and criteria that delineate shallow and nonshallow arches are proposed. Comparisons with finite element results demonstrate that the solutions and approximations are accurate. It is found that the existence of antisymmetric bifurcation buckling loads is not a sufficient condition for antisymmetric bifurcation buckling to take place.

DOI: 10.1061/(ASCE)0733-9399(2002)128:7(710)

CE Database keywords: Bifurcation; Buckling; Concentrated loads; Arches.

Introduction

This paper is concerned with the in-plane elastic stability of arches subjected to a central concentrated load (Fig. 1). When the lateral displacements and twist rotations of an arch are fully restrained, the arch (Fig. 1) may buckle in an in-plane antisymmetric bifurcation mode [Fig. 2(a)] or in an in-plane symmetric snap-through mode [Fig. 2(b)].

The classical methods for predicting elastic buckling loads consider bifurcation from a prebuckling equilibrium path to an orthogonal buckling path (Timoshenko and Gere 1961; Vlasov 1961; Simites 1976; Trahair and Bradford 1998). The analysis of prebuckling equilibrium is linear and so the stress resultants can be linearized. Nonlinearities are not considered in the prebuckling analysis and so their effects on buckling cannot be included in the buckling analysis. These classical methods are suitable for the elastic buckling analysis of columns, beams, and frames. For example, in the case of a column, the prebuckling or primary equilibrium path involves linear axial deformation only, and so the column is under a uniform axial compressive action in its prebuckling configuration. The flexural buckling path that is

orthogonal to the prebuckling path at the point of bifurcation involves primarily transverse deflections. In the case of an arch, however, the prebuckling equilibrium path involves both axial and transverse deformations and so the arch is under both axial compression and bending in its prebuckling configuration. Moreover, the transverse deformations are significant prior to buckling and the prebuckling elastic behavior may become nonlinear, so that these effects necessarily need to be accounted for in the in-plane buckling analysis of an arch.

Closed form solutions for the classical buckling load for pin-ended and fixed circular arches subjected to a radial load uniformly distributed around the arch axis are given in several publications such as Timoshenko and Gere (1961), Vlasov (1961), Simites (1976), and Pi and Bradford (2002). However, for arbitrary loading, numerical methods such as finite element (FE) methods are often used for the prebuckling linear elastic analysis, and an eigenvalue formulation is then invoked to determine the buckling loads (Rajasekaran and Padmanabhan 1989; Kang and Yoo 1994). The discrepancies between the classical buckling loads and test results has been realized by a number of researchers (Gjelsvik and Bodner 1962; Dickie and Broughton 1971), and discrepancies between the numerical eigenvalue-based results and the test results have also been identified (Pi and Trahair 1998; Pi and Bradford 2001). These discrepancies arise owing to the linearization of the prebuckling path. The buckling of sinusoidal shallow arches was studied by Timoshenko and Gere (1961) and Simites (1976). Gjelsvik and Bodner (1962) used an energy method to investigate the instability of fixed shallow circular arches of rectangular solid cross section subjected to central point loading, and approximate solutions were obtained. Schreyer and Masur (1966) performed an exact analysis for shallow circular arches and derived analytical solutions, but their analysis was limited to fixed arches of a rectangular solid cross section and their solutions for the symmetric buckling mode were very complicated. Dickie and Broughton (1971) used a series method to

¹Professor, School of Civil and Environmental Engineering, Univ. of New South Wales, Sydney 2052, NSW, Australia.

²Senior Lecturer, School of Civil and Environmental Engineering, Univ. of New South Wales, Sydney 2052, NSW, Australia.

³Senior Research Fellow, School of Civil and Environmental Engineering, Univ. of New South Wales, Sydney 2052, NSW, Australia.

Note. Associate Editor: Guillermo D. Hahn. Discussion open until December 1, 2002. Separate discussions must be submitted for individual papers. To extend the closing date by one month, a written request must be filed with the ASCE Managing Editor. The manuscript for this paper was submitted for review and possible publication on December 13, 2000; approved on September 18, 2001. This paper is part of the *Journal of Engineering Mechanics*, Vol. 128, No. 7, July 1, 2002. ©ASCE, ISSN 0733-9399/2002/7-710-719/\$8.00+\$5.00 per page.

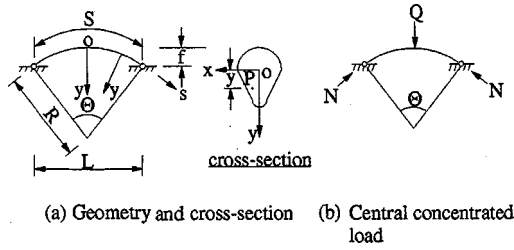


Fig. 1. Arches and loading

study the buckling of shallow circular pin-ended and fixed arches. However, their study was again confined to rectangular solid cross sections and only approximate numerical solutions were given. In addition to a rectangular cross section, other shapes such as I sections and rectangular hollow sections are widely used for arches, as are a number of materials. Most of the pertinent research findings have been summarized in *Handbook* (1971) and *Guide to stability design* (1976, 1988). Pi and Bradford (2002) recently studied the in-plane elastic stability of circular arches with a symmetric cross section and subjected to a radial load uniformly distributed around the arch axis. This analysis incorporated a nonlinear formulation for the prebuckling configuration. Research using numerical methods for the in-plane buckling of arches has been extensive in recent years (Noor and Peters 1981; Stolarski and Belytschko 1982; Calhoun and DaDeppo 1983; Elias and Chen 1988; Wen and Suhendro 1991; Pi and Trahair 1998). It has been shown (Wen and Suhendro 1991; Pi and Trahair 1998) that the assumption of a linear prebuckling configuration with an eigenvalue approach for determining the buckling loads is not suitable for the in-plane elastic buckling analysis of shallow arches, and nonlinear analysis needs to be deployed. It is not widely recognized that classical buckling theory cannot correctly predict the in-plane buckling load of shallow arches and this issue is addressed herein.

The purposes of this paper are: to investigate analytically the in-plane elastic stability of both pin-ended and fixed circular arches with a symmetric cross section and subjected to a central concentrated load; to use a virtual work procedure to establish the nonlinear equilibrium conditions for shallow arches; to perform a nonlinear buckling analysis to obtain analytical solutions for the buckling load of shallow arches; and to propose approximations to the symmetric buckling load of shallow arches and nonshallow fixed arches and for the antisymmetric buckling load of nonshallow pin-ended arches.

Nonlinear In-Plane Equilibrium

Differential Equilibrium Equations

Because classical buckling theory does not account for the often significant effects of prebuckling deformation and nonlinearity on

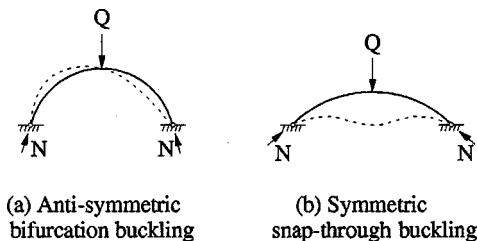


Fig. 2. Buckling modes

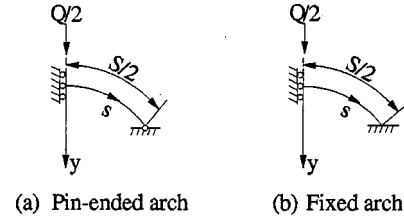


Fig. 3. Half of arches

buckling, it cannot be used to predict accurately the in-plane buckling of shallow arches. A virtual work procedure is used in this section to investigate the in-plane buckling of shallow arches by accounting for the effects of prebuckling deformations and nonlinearity. The FE results reported by Pi and Trahair (1998) demonstrated that the nonlinearity is due to large transverse deformation and that the axial displacements w of shallow arches are quite small prior to buckling, so that their effects on the radial deformation may be ignored without error. Thus the longitudinal normal strain of a point P can be written as

$$\epsilon_P = \epsilon_m + \epsilon_b \quad (1)$$

where the membrane strain ϵ_m and the bending strain ϵ_b are given by

$$\epsilon_m = w' - \frac{v}{R} + \frac{1}{2}(v')^2 \quad \text{and} \quad \epsilon_b = -yv'' \quad (2)$$

where the term $(v')^2/2$ is used to account for the large transverse deformation and it is the source of nonlinearity.

The nonlinear in-plane equilibrium equations for a shallow arch subjected to a central concentrated load Q can be derived from the principle of virtual work that requires

$$\delta U = \int_V \delta \epsilon \sigma dV - Q \delta v_0 = 0 \quad (3)$$

for all sets of kinematically admissible virtual displacements δw and δv , where v_0 = central radial displacement.

Because the deformations of an arch prior to buckling are symmetric under a central concentrated load, half of the arch can be used for the derivation as shown in Fig. 3, in which case the virtual work statement of Eq. (3) can be written as

$$\int_0^{S/2} \left[EA \left(\delta w' - \frac{\delta v}{R} + v' \delta v' \right) \epsilon_m + EI_x v'' \delta v'' \right] ds - \frac{Q}{2} \delta v_0 = 0 \quad (4)$$

Integrating Eq. (4) by parts leads to the differential equilibrium equations

$$-EA \epsilon'_m = 0 \quad (5)$$

for the axial direction and

$$EI_x v^{iv} - EA v'' \epsilon_m - EA \frac{\epsilon_m}{R} - EA v' \epsilon'_m = 0 \quad (6)$$

for the radial direction.

When the right-hand half of an arch is used, integrating Eq. (4) also leads to the boundary conditions for a pin-ended arch

$$v' = 0 \quad \text{at} \quad s = 0 \quad (7)$$

which represents that the slope of the midsurface of the arch is equal to zero

$$EI_x v''' - \frac{Q}{2} = 0 \quad \text{at } s=0 \quad (8)$$

which represents that the shear force at the midsurface of the arch is equal to zero, and

$$EI_x v'' = 0 \quad \text{at } s=S/2 \quad (9)$$

which represents that the bending moment at the pin-end ($s=S/2$) vanishes. In addition, the displacement boundary condition at $s=S/2$ for the right-hand half of a pin-ended arch is $v=0$.

The boundary conditions for a fixed arch can be obtained in the same way and are identical to Eqs. (7) and (8). The displacement boundary conditions at $s=S/2$ for the right-hand half of a fixed arch are $v=v'=0$.

When the left-hand half of an arch is used, the boundary condition (8) becomes

$$EI_x v''' + \frac{Q}{2} = 0 \quad \text{at } s=0 \quad (10)$$

the boundary condition (9) for a pin-ended arch becomes

$$EI_x v'' = 0 \quad \text{at } s=-S/2 \quad (11)$$

and the corresponding displacement boundary conditions at $s=-S/2$ are $v=0$ for a pin-ended arch and $v=v'=0$ for a fixed arch.

From Eq. (5), the membrane strain ϵ_m is constant and can be written as

$$\epsilon_m = -\frac{\bar{N}}{EA} \quad (12)$$

where \bar{N} =actual axial compression force in the arch.

Introducing a parameter μ defined by

$$\mu^2 = \frac{\bar{N}}{EI_x} \quad (13)$$

and substituting Eqs. (5), (12), and (13) into Eq. (6) leads to the differential equilibrium equation for the radial direction as

$$\frac{v^{iv}}{\mu^2} + v'' = \frac{-1}{R} \quad (14)$$

Nonlinear Equilibrium Conditions for Pin-Ended Arch

The radial displacements v , which satisfy the boundary conditions (7)–(9), (10), (11), and $v=0$ at $s=\pm S/2$, can be obtained by solving Eq. (14) as

$$v = \frac{1}{\mu^2 R} \left\{ \frac{\cos(\mu S/2) - \cos(\mu s)}{\cos(\mu S/2)} + \frac{1}{2} [(\mu S/2)^2 - (\mu s)^2] \right\} + \frac{Q}{2EI_x \mu^3} \{ \tan(\mu S/2) \cos(\mu s) - (\mu S/2) - H(s) [\sin(\mu s) - (\mu s)] \} \quad (15)$$

where the step function $H(s)$ is defined as

$$H(s) = \begin{cases} -1 & \text{when } s < 0 \\ 1 & \text{when } s \geq 0 \end{cases} \quad (16)$$

The nonlinear equilibrium conditions for shallow arches can be established by considering that the constant membrane strain

given by Eq. (12) should be equal to the average membrane strain over the arch length S calculated from Eq. (2), so that

$$-\frac{\bar{N}}{EA} = \frac{1}{S} \int_{-S/2}^{S/2} \left(w' - \frac{v}{R} + \frac{v'^2}{2} \right) ds \quad (17)$$

Using the boundary conditions $w=0$ at $s=\pm S/2$, it is clear that

$$\frac{1}{S} \int_{-S/2}^{S/2} w' ds = 0 \quad (18)$$

and from Eq. (13), the left-hand side of Eq. (17) can be rewritten as

$$-\frac{\bar{N}}{EA} = -\frac{\bar{N}}{EI_x} \frac{I_x}{A} = -\mu^2 r_x^2 \quad (19)$$

where r_x =radius of gyration of the cross section about the major principal axis given by $r_x = \sqrt{I_x/A}$.

Considering Eq. (18) and substituting Eqs. (15) and (19) into Eq. (17) leads to the nonlinear equilibrium condition for pin-ended shallow arches given by

$$A_1 \bar{Q}^2 + B_1 \bar{Q} + C_1 = 0 \quad (20)$$

where the coefficients A_1 , B_1 , and C_1 are given by

$$A_1 = \frac{1}{4(\mu S/2)^4} \left[3 - 3 \frac{\tan(\mu S/2)}{\mu S/2} + \tan^2(\mu S/2) \right] \quad (21)$$

$$B_1 = \frac{1}{(\mu S/2)^4} \left[\frac{1}{\cos(\mu S/2)} - 1 - \frac{(\mu S/2) \tan(\mu S/2)}{2 \cos(\mu S/2)} \right] \quad (22)$$

$$C_1 = \left(\frac{\mu S}{2\lambda_s} \right)^2 + D_1 \quad (23)$$

with

$$D_1 = \frac{1}{4(\mu S/2)^2} \left[1 + \tan^2(\mu S/2) - \frac{\tan(\mu S/2)}{(\mu S/2)} - \frac{2(\mu S/2)^2}{3} \right] \quad (24)$$

λ_s =modified slenderness for an arch defined by

$$\lambda_s = \frac{\Theta}{2} \frac{(S/2)}{r_x} = \frac{S^2}{4r_x R} \quad (25)$$

and \bar{Q} =dimensionless load defined by

$$\bar{Q} = \frac{\pi^2 Q}{\Theta N_P} \quad (26)$$

and in which N_P =second mode buckling load of a pin-ended column about its major axis under uniform axial compression given by

$$N_P = \frac{\pi^2 EI_x}{(S/2)^2} \quad (27)$$

Nonlinear Equilibrium Conditions for Fixed Arch

Following the previous procedure, the solution of Eq. (14) for fixed arches, which satisfies the boundary conditions (7), (8), (10), and $v=v'=0$ at $s=\pm S/2$, can be obtained as

$$v = \frac{1}{\mu^2 R} \left\{ \frac{(\mu S/2)[\cos(\mu S/2) - \cos(\mu S)]}{\sin(\mu S/2)} + \frac{1}{2}[(\mu S/2)^2 - (\mu s)^2] \right\} + \frac{Q}{2EI_x \mu^3} \{ \tan(\mu S/4)[\cos(\mu s) + 1] + H(s)[(\mu s) - \sin(\mu s)] - (\mu S/2) \} \quad (28)$$

Considering Eq. (18) and substituting Eqs. (19) and (28) into Eq. (17) leads to the nonlinear equilibrium condition for fixed arches given by

$$A_2 \bar{Q}^2 + B_2 \bar{Q} + C_2 = 0 \quad (29)$$

where the coefficients A_2 , B_2 , and C_2 are given by

$$A_2 = \frac{1}{4(\mu S/2)^4} \left[3 + \tan^2\left(\frac{\mu S/2}{2}\right) - \frac{6}{(\mu S/2)} \tan\left(\frac{\mu S/2}{2}\right) \right] \quad (30)$$

$$B_2 = \frac{1}{2(\mu S/2)^3} \left[\tan\left(\frac{\mu S/2}{2}\right) - \frac{\mu S/2}{2} - \frac{(\mu S/2)}{2} \tan^2\left(\frac{\mu S/2}{2}\right) \right] \quad (31)$$

$$C_2 = \left(\frac{\mu S}{2\lambda_2}\right)^2 + \frac{1}{4(\mu S/2)^2} \left[(\mu S/2)^2 \cot^2(\mu S/2) - (\mu S/2) \cot(\mu S/2) + \frac{(\mu S/2)^2}{3} \right] \quad (32)$$

and the dimensionless load \bar{Q} is defined by

$$\bar{Q} = \frac{(1.4303\pi)^2 Q}{\Theta N_F} \quad (33)$$

in which N_F = second mode buckling load of a fixed column about its major axis under uniform axial compression given by

$$N_F = \frac{(1.4303\pi)^2 EI_x}{(S/2)^2} \quad (34)$$

Buckling Analysis

Buckling Equations

For the stability of an equilibrium position defined by v and w to be neutral, it is required that

$$\delta^2 U = 0 \quad (35)$$

for the buckling displacements $v_b = \delta v$ and $w_b = \delta w$ that take place from the prebuckling equilibrium position v and w to the adjacent buckling equilibrium position $v + v_b$ and $w + w_b$ under constant loads.

The neutral equilibrium condition of Eq. (35) is equivalent to a variation of the virtual work (3) as

$$\int_{-S/2}^{S/2} \left[EA \left(w'_b \epsilon_{mb} - \frac{v_b \epsilon_{mb}}{R} + v' v'_b \epsilon_{mb} + v_b'^2 \epsilon_m \right) + EI_x v_b''^2 \right] ds = 0 \quad (36)$$

where ϵ_{mb} = membrane strain during buckling given by

$$\epsilon_{mb} = \delta \epsilon_m = w'_b - \frac{v_b}{R} + v' v'_b \quad (37)$$

The left-hand side of Eq. (36) can be considered as a function of the buckling displacements v_b and w_b . The buckling displacements that make the functional stationary satisfy the Euler–Lagrange equations of variational calculus, from which and by considering Eqs. (12) and (13), the buckling differential equilibrium equation in the axial direction can be obtained as

$$\epsilon'_{mb} = 0 \quad (38)$$

from which the membrane strain ϵ_{mb} during buckling is a constant; and the buckling differential equilibrium equation in the radial direction can be obtained as

$$v_b^{iv} + \mu^2 v_b'' = \frac{\epsilon_{mb}}{r_x^2} \left(\frac{1}{R} + v'' \right). \quad (39)$$

Buckling of Pin-Ended Shallow Arch

For antisymmetric bifurcation buckling, the buckling displacement v_b is antisymmetric while the prebuckling displacement v is symmetric, so that the terms v_b and $v' v'_b$ are antisymmetric and their integrals within the interval $[-S/2, S/2]$ vanish. In addition, the boundary conditions require that $w_b = 0$ at $s = \pm S/2$, so that the average strain ϵ_{mb} during buckling is obtained as

$$\epsilon_{mb} = \frac{1}{S} \int_{-S/2}^{S/2} \epsilon_{mb} ds = \frac{1}{S} \int_{-S/2}^{S/2} \left(w'_b - \frac{v_b}{R} + v' v'_b \right) ds = 0 \quad (40)$$

Substituting $\epsilon_{mb} = 0$ into Eq. (39) leads to the linear homogeneous differential equation for antisymmetric buckling of a shallow arch given by

$$\frac{v_b^{iv}}{\mu^2} + v_b'' = 0 \quad (41)$$

The solution of Eq. (41) that satisfies the boundary conditions $v_b = 0$ at $s = \pm S/2$ is

$$v_b = C \left[\sin(\mu s) - \frac{s \sin(\mu S/2)}{S/2} \right] \quad (42)$$

where C = amplitude parameter.

For a pin-ended arch, using the boundary conditions $v_b'' = 0$ at $s = \pm S/2$, Eq. (42) leads to

$$\sin(\mu S/2) = 0 \quad (43)$$

whose fundamental solution is

$$\frac{\mu S}{2} = \pi \quad (44)$$

so that, with the use of Eq. (13), the corresponding actual axial compression \bar{N} in a pin-ended arch during bifurcation antisymmetric buckling is

$$\bar{N} = \frac{\pi^2 EI_x}{(S/2)^2} \quad (45)$$

which is equal to the familiar second mode buckling load N_p of a pin-ended column under uniform compression.

Substituting Eq. (44) into the nonlinear equilibrium condition (20) leads to

$$3\bar{Q}_{sb}^2 - 8\bar{Q}_{sb} + \pi^2 - \frac{2\pi^4}{3} + \frac{4\pi^6}{\lambda_s^2} = 0 \quad (46)$$

Solving Eq. (46) for \bar{Q}_{sb} leads to the antisymmetric buckling load of a pin-ended shallow arch given by

$$\bar{Q}_{sb} \approx 1.33 \pm 4.5 \sqrt{1 - 0.65 \frac{\pi^4}{\lambda_s^2}} \quad (47)$$

When $\lambda_s \geq \sqrt{0.65\pi^2} \approx 7.96$, a real antisymmetric buckling solution (47) exists, so that antisymmetric buckling of the pin-ended arch may occur.

For the symmetric snap-through buckling of a pin-ended arch, the buckling displacement v_b is symmetric. Substituting Eq. (15) into Eq. (39) leads to the buckling equilibrium equation

$$\frac{v_b^{iv}}{\mu^2} + v_b'' = \frac{\epsilon_{mb}}{\mu^2 r_x^2} \frac{1}{R} \left\{ \frac{\cos(\mu s)}{\cos(\mu S/2)} - \frac{\bar{Q}[\tan(\mu S/2)\cos(\mu s) - H(s)\sin(\mu s)]}{(\mu S/2)} \right\} \quad (48)$$

The solution of Eq. (48), which satisfies the boundary conditions $v_b = v_b'' = 0$ at $s = S/2$, is

$$v_b = \frac{1}{\mu^2 r_x^2} \frac{\epsilon_{mb}}{\mu^2 R} \left\{ \frac{(\mu S/2)\sin(\mu S/2)\cos(\mu s) - (\mu s)\sin(\mu s)\cos(\mu S/2)}{2 \cos^2(\mu S/2)} + 1 - \frac{\cos(\mu s)}{\cos(\mu S/2)} \right. \\ \left. + \frac{\bar{Q}}{2} \left[\frac{(\mu s)\sin(\mu s)\sin(\mu S/2)}{\mu S/2 \cos(\mu S/2)} + \left(\frac{\tan(\mu S/2)}{(\mu S/2)} - \frac{1}{\cos^2(\mu S/2)} \right) \cos(\mu s) + H(s) \left(\frac{(\mu s)\cos(\mu s)}{(\mu S/2)} - \frac{\sin(\mu s)}{(\mu S/2)} \right) \right] \right\} \quad (49)$$

The average buckling membrane strain of Eq. (37) over the arch length S is equal to the constant buckling membrane strain ϵ_{mb} , which leads to an equation for the relationship between the dimensionless buckling load \bar{Q}_{ss} and the dimensionless parameter $\mu S/2$ during symmetric snap-through buckling given by

$$A_3 \bar{Q}_{ss}^2 + B_3 \bar{Q}_{ss} + C_3 = 0 \quad (50)$$

where

$$A_3 = \frac{A_1}{2} + \frac{\tan^2(\mu S/2)}{4(\mu S/2)^4} - \frac{\tan(\mu S/2) + \tan^3(\mu S/2)}{4(\mu S/2)^3} \quad (51)$$

$$B_3 = B_1 + \frac{1 + \sin^2(\mu S/2)}{4(\mu S/2)^2 \cos^3(\mu S/2)} - \frac{\sin(\mu S/2)}{4(\mu S/2)^3 \cos^2(\mu S/2)} \quad (52)$$

and

$$C_3 = \frac{3D_1}{2} + \frac{(\mu S/2) - \tan(\mu S/2) - \tan^3(\mu S/2)}{4(\mu S/2)} - \left(\frac{\mu S}{2\lambda} \right)^2 \quad (53)$$

and where A_1 , B_1 , and D_1 are given by Eqs. (21), (22), and (24).

For a given value of μ , a solution for the symmetric snap-through buckling load \bar{Q}_{ss} and the corresponding value of λ_s can be obtained by solving Eqs. (20) and (50) simultaneously. However, the value of λ_s rather than the value of μ is usually known for a shallow arch. In this case, an iterative process needs to be used to obtain a solution of \bar{Q}_{ss} by solving Eqs. (20) and (50) simultaneously.

The value of the modified slenderness λ_s that defines a switch between the buckling modes can be found when $\bar{Q}_{ss} = \bar{Q}_{sb}$ at $\mu S/2 = \pi$, which leads to $\lambda_s \approx 9.80$. When $\lambda_s > 9.80$, a pin-ended arch may buckle in an antisymmetric mode, but when $7.96 \leq \lambda_s \leq 9.80$, both symmetric and antisymmetric buckling may occur. It will be shown next that symmetric buckling occurs first and that antisymmetric buckling occurs on the descending branch of the load-displacement curve. When the modified slenderness $\lambda_s < 7.96$, a pin-ended arch may buckle only in a symmetric mode.

Because the iterative solution process for the symmetric buckling load of an arch is complicated, an approximation for the symmetric buckling load of a pin-ended arch whose modified slenderness $\lambda_s \leq 9.80$ is proposed as

$$\bar{Q}_{ss} \approx 1 + 0.03\lambda_s^2 \quad (54)$$

The lowest symmetric buckling load for a pin-ended arch can be obtained from Eq. (20) as (Bradford et al. 2000)

$$\lim_{\mu S/2 \rightarrow \pi/2} \bar{Q} = \frac{\pi}{2} \quad (55)$$

In this case, the actual axial compression \bar{N} in the pin-ended arch is related to the lowest symmetric snap-through buckling load \bar{Q}_{ss} as

$$\bar{Q}_s = \frac{N_P \Theta}{2\pi} = \frac{2\Theta \bar{N}}{\pi} \quad (56)$$

From Eq. (15), the central radial displacement v_c of a pin-ended arch ($s=0$) is

$$v_c = \frac{1}{v^2 R} \left\{ 1 - \frac{1}{\cos(\mu S/2)} + \frac{(\mu S/2)^2}{2} - \frac{\bar{Q}[\tan(\mu S/2) - (\mu S/2)]}{(\mu S/2)} \right\} \quad (57)$$

Hence the corresponding central radial displacement v_c at $\bar{Q}_{ss} = \pi/2$ can be obtained from Eq. (57) as (Bradford et al. 2000)

$$\lim_{\mu S/2 \rightarrow \pi/2} v_c = \frac{S^2}{\pi^2 R} \left(1 - \frac{2}{\pi} + \frac{\pi^2}{8} - \frac{\pi}{2} \right. \\ \left. \pm \sqrt{\frac{4}{\pi^2} + \frac{8}{\pi} + \frac{\pi^2}{6} - 3 - \frac{\pi^4}{4\lambda_s^2}} \right) \quad (58)$$

The value of the central radial displacement v_c is real when $(4/\pi^2) + (8/\pi) + (\pi^2/6) - 3 - (\pi^4/4\lambda_s^2) \geq 0$, that is when $\lambda_s \geq 3.91$. When $\lambda_s < 3.91$, a pin-ended arch does not buckle.

Solution (47) for antisymmetric buckling and the approximation (54) for symmetric buckling of a pin-ended arch are com-

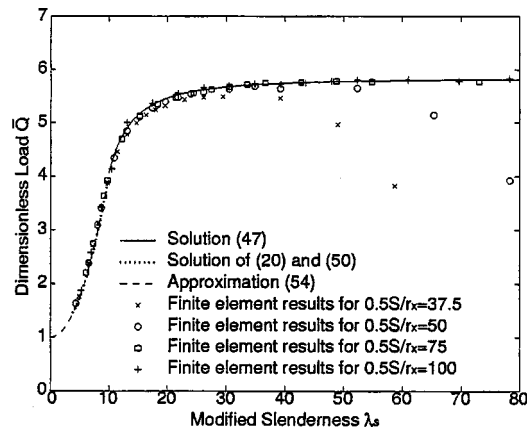


Fig. 4. Buckling of pin-ended arches against slenderness

pared with FE predictions in Figs. 4 and 5. The symmetric buckling solution for arches with modified slenderness $\lambda_s \leq 9.80$ obtained by simultaneously solving Eqs. (20) and (50) is also shown in Fig. 4. Fig. 4 shows the variation of the dimensionless buckling load \bar{Q} with the modified slenderness λ_s , while Fig. 5 shows the variation of the dimensionless buckling load \bar{Q} with the included angle Θ . The FE package *ABAQUS* (1998) and the FE program developed by Pi and Trahair (1998) were used for the numerical analysis, and the results of *ABAQUS* are identical to those of Pi and Trahair. In the FE analysis, an I-section, a rectangular hollow section, and a rectangular solid cross section were used. The dimensionless of the I-section are: the overall depth $D=0.2613$ m, the flange width $B=0.151$ m, the flange thickness $t_f=0.0123$ m, and the web thickness $t_w=0.0077$ m. The dimensions of the rectangular hollow section are: the overall height $D=0.4$ m, the width $B=0.25$ m, and the wall-thickness $t=0.003$ m. The dimensionless of the rectangular solid cross section are: the height $D=0.005$ m and the width $B=0.010$ m. The Young's modulus of elasticity was assumed to be equal to $E=200,000$ MPa for the three sections.

It can be observed from Fig. 4 that the approximation (54) is almost identical to the solution from Eqs. (20) and (50) for symmetric buckling of pin-ended arches with the modified slenderness $\lambda_s \leq 9.80$. Both of these agree extremely well with the FE predictions. The solution (47) for antisymmetric buckling almost coincides with the FE results for pin-ended arches with the modi-

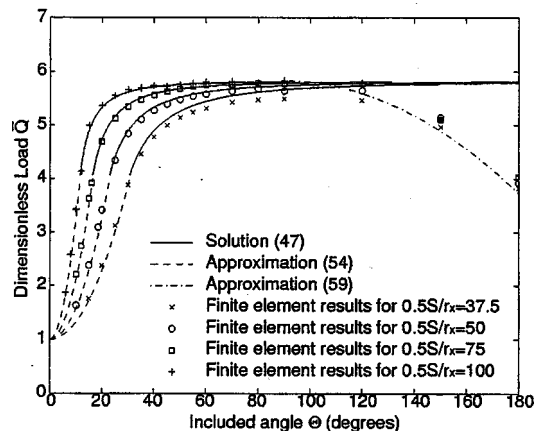


Fig. 5. Buckling of pin-ended arches against included angle

fied slenderness $40 \geq \lambda_s \geq 9.80$. It can be seen from Fig. 5 that the solution (47) and the approximation (54) agree very well with the FE results when the included angle $\Theta \leq 90^\circ (\pi/2)$.

When the included angle $\Theta \geq 90^\circ (\pi/2)$, the solution (47) approaches a certain value ($\bar{Q}_{sb}=5.83$) with the increase of the modified slenderness and of the included angle Θ , and tends to be higher than the FE predictions. The included angle $\Theta = 90^\circ (\pi/2)$ can be used as a criterion for distinguishing between shallow and nonshallow pin-ended arches based on their in-plane instability under a central concentrated load. The antisymmetric buckling load of nonshallow arches [$\Theta \geq 90^\circ (\pi/2)$] can be approximated by

$$\bar{Q}_{sb} = 5.83 - 0.85 \left(\Theta - \frac{\pi}{2} \right)^2 \quad (59)$$

where the included angle Θ is expressed in radians. Fig. 5 shows that the approximation (59) agrees very well with the FE results.

Buckling of Fixed Shallow Arch

For antisymmetric buckling of fixed shallow arches, the use of the boundary condition $v_b = v'_b = 0$ at $s = \pm S/2$ in Eq. (42) produces

$$\tan(\mu S/2) = \mu S/2 \quad (60)$$

The lowest solution of Eq. (60) is

$$\frac{\mu S}{2} \approx 1.4303\pi \quad (61)$$

so that, with the use of Eq. (13), the corresponding actual axial compression \bar{N} in a fixed arch at antisymmetric buckling is

$$\bar{N} \approx \frac{(1.4303\pi)^2 EI_x}{(S/2)^2} \quad (62)$$

which is equal to the second mode buckling load N_F of a fixed column under uniform compression.

Substituting Eqs. (60) and (61) into Eq. (29) leads to

$$6.22\bar{Q}_{sb}^2 - 13.98 \times (1.4303\pi) \bar{Q}_{sb} + \frac{(1.4303\pi)^4}{3} + \frac{4 \times (1.4303\pi)^6}{\lambda_s^2} = 0 \quad (63)$$

and solving Eq. (63) for \bar{Q}_{sb} leads to the antisymmetric buckling load of fixed shallow arches given by

$$\bar{Q}_{sb} \approx 1.4303\pi \times \left(1.12 \pm 0.18 \sqrt{1 - 15 \frac{\pi^4}{\lambda_s^2}} \right) \quad (64)$$

When $\lambda_s \geq \sqrt{15}\pi^2 (\approx 38.15)$, a real antisymmetric buckling solution (64) exists, so that antisymmetric buckling of the fixed arch may occur. Solution (64) can be reduced to that of Schreyer and Masur (1966) for fixed shallow arches with a rectangular solid cross section subjected to a central concentrated load.

For symmetric snap-through buckling of a fixed arch, substituting Eq. (28) into Eq. (39) leads to the buckling equilibrium equation

$$\frac{v_b^{iv}}{\mu^2} + v_b'' = \frac{\epsilon_{mb}}{\mu^2 r_x^2} \frac{1}{R} \left\{ \frac{(\mu S/2) \cos(\mu s)}{\sin(\mu S/2)} - \frac{\bar{Q} [\tan(\mu S/4) \cos(\mu s) - H(s) \sin(\mu s)]}{(\mu S/2)} \right\} \quad (65)$$

The solution of Eq. (65), which satisfies the boundary conditions $v_b = v_b' = 0$ at $s = S/2$, is

$$v_b = \frac{\epsilon_{mb}}{\mu^4 r_x^2 R} \left\{ \frac{(\mu S/2) [\cos(\mu S/2) - \cos(\mu s) - (\mu s) \sin(\mu s)]}{2 \sin(\mu S/2)} + \frac{(\mu S/2)^2 [1 - \cos(\mu S/2) \cos(\mu s)]}{2 \sin^2(\mu S/2)} \right. \\ \left. - \frac{\bar{Q}}{2} \left[\frac{\cos(\mu S/2) - \cos(\mu s) + \cos(\mu S/2) \cos(\mu s) - 1}{(\mu S/2) \sin(\mu S/2)} + \frac{[1 - \cos(\mu S/2)][1 + \cos(\mu s)]}{\sin^2(\mu S/2)} - \frac{(\mu s) \sin(\mu s) [1 - \cos(\mu S/2)]}{(\mu S/2) \sin(\mu S/2)} \right] \right. \\ \left. - \frac{H(s) [(\mu s) \cos(\mu s) - \sin(\mu s)]}{(\mu S/2)} \right\} \quad (66)$$

The average buckling membrane strain of Eq. (37) over the arch length S is equal to the constant buckling membrane strain ϵ_{mb} , which leads to an equation for the relationship between the dimensionless load \bar{Q} and the dimensionless parameter $\mu S/2$ during symmetric snap-through buckling given by

$$A_4 \bar{Q}^2 + B_4 \bar{Q} + C_4 = 0 \quad (67)$$

where

$$A_4 = \frac{1}{(\mu S/2)^3} \left\{ \frac{3 \tan(\mu S/4)}{4 \sin(\mu S/2)} - \frac{3 \sin(\mu S/2)}{8 (\mu S/2)^2} - \frac{\tan^2(\mu S/4)}{4 \sin(\mu S/2)} \right. \\ \left. - \frac{\tan^3(\mu S/4) \sin^2(\mu S/2)}{4 (\mu S/2)^2} - \frac{\tan(\mu S/4) \sin^2(\mu S/2)}{8 (\mu S/2)} \right. \\ \left. - \frac{\tan^2(\mu S/4) \cos(\mu S/2)}{8 (\mu S/2)} \right\} \quad (68)$$

$$B_4 = \frac{\tan(\mu S/4)}{4 (\mu S/2)^3} + \frac{\tan^2(\mu S/4)}{4 (\mu S/2) \sin(\mu S/2)} - \frac{\tan(\mu S/4)}{4 (\mu S/2)^2 \sin(\mu S/2)} \quad (69)$$

and

$$C_4 = \frac{(\mu S/2) \cos(\mu S/2)}{4 \sin^3(\mu S/2)} - \frac{1}{8 \sin^2(\mu S/2)} - \frac{\cot(\mu S/2)}{(\mu S/2)} - \left(\frac{\mu S}{2 \lambda_s} \right)^2 \quad (70)$$

Alternatively, the symmetric buckling of pin-ended and fixed arches can be obtained by finding the maximum value of \bar{Q} by differentiating Eq. (20) for pin-ended arches or by differentiating Eq. (29) for fixed arches using

$$\frac{d\bar{Q}}{d(\mu S/2)} = 0 \quad (71)$$

However, implementing this process becomes very complicated and this is not pursued further.

For a given value of μ , a solution for the symmetric snap-through buckling load \bar{Q}_{ss} and the corresponding value of λ_s can be obtained by solving Eqs. (29) and (67) simultaneously. However, again the value of λ_s rather than the value of μ is usually known for a specific shallow arch. In this case, an iterative process again needs to be used to obtain a solution for Q_s by solving Eqs. (29) and (67) simultaneously.

The value of the modified slenderness λ_s for distinguishing between the buckling modes may be found when $\bar{Q}_{ss} = \bar{Q}_{sb}$ at $\mu S/2 = 1.4303\pi$. However, there is no real-value solution for λ_s . This indicates that symmetric buckling governs the buckling of fixed arches subjected to a central concentrated load. It will be shown next that symmetric buckling occurs first and that antisymmetric buckling occurs in the unstable region, i.e., on the descending branch of the load-displacement curve when the modified slenderness $\lambda_s \geq 38.15$. When the modified slenderness $\lambda_s < 38.15$, the fixed arch may buckle only in a symmetric mode.

Because the solution processes for a symmetric buckling mode are complicated, approximations for the symmetric buckling load of fixed arches are proposed as

$$\bar{Q}_{ss} \approx 3.30 + 0.17\lambda_s - 0.002\lambda_s^2 \quad \text{for } 11 < \lambda_s \leq 38 \quad (72)$$

and

$$\bar{Q}_{ss} \approx 5.88 + 0.03\lambda_s - 0.0001\lambda_s^2 \quad \text{for } \lambda_s > 38 \quad (73)$$

The lowest symmetric buckling load for a fixed arch can be obtained from Eq. (29) as (Bradford et al. 2000)

$$\lim_{\mu S/2 \rightarrow \pi} \bar{Q} = \frac{\pi^2}{2} \quad (74)$$

In this case, the actual axial compression \bar{N} in a fixed arch is relate to the lowest symmetric snap-through buckling load Q_{ss} as

$$Q_{ss} = \frac{N_F \Theta}{2 \times (1.4303\pi)^2} = \frac{\bar{N} \Theta}{2} \quad (75)$$

From Eq. (28), the central radial displacement v_c of the fixed arch ($s=0$) is

$$v_c = \frac{1}{\mu^2 R} \left\{ \frac{(\mu S/2) [\cos(\mu S/2) - 1]}{\sin(\mu S/2)} + \frac{(\mu S/2)^2}{2} \right. \\ \left. + \frac{\bar{Q} [2 \tan(\mu S/4) - (\mu S/2)]}{(\mu S/2)} \right\} \quad (76)$$

Thus the corresponding central radial displacement v_c at $\bar{Q}_{ss} = \pi^2/2$ can be obtained from Eq. (76) as (Bradford et al. 2000)

$$\lim_{\mu S/2 \rightarrow \pi} v_c = \frac{S^2}{\pi^2 R} \left(1 \pm \sqrt{1 - \frac{\pi^2}{48} - \frac{\pi^4}{\lambda_s^2}} \right) \quad (77)$$

The value of the central radial displacement v_c is real when 1

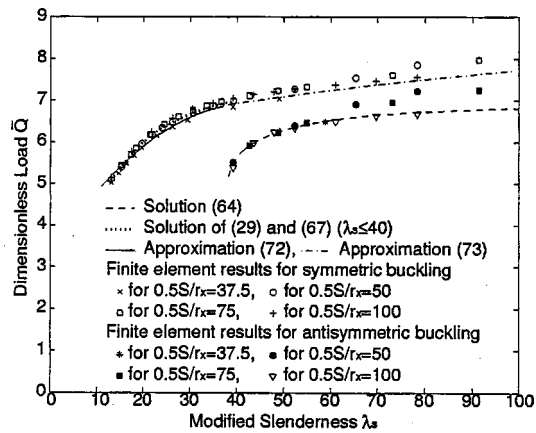


Fig. 6. Buckling of fixed arches against slenderness

$-(\pi^2/48) - (\pi^4/\lambda_s^2) \geq 0$, that is when $\lambda_s \geq 1.122\pi^2 (\approx 11.07)$. When the modified slenderness $\lambda_s \leq 11.07$, a fixed shallow arch does not buckle.

FE methods (ABAQUS 1998; Pi and Trahair 1998) have been used to investigate the buckling behavior of fixed arches under a central concentrated load. In the FE analysis, the cross sections and material properties are the same as those used for the pin-ended arches. The results confirm that symmetric buckling dominates. The points of antisymmetric bifurcation buckling are located in the unstable region, i.e., on the descending branch of the load-deflection curve and so antisymmetric bifurcation buckling may not really occur. The approximations (72) and (73) for symmetric buckling are compared with the FE results in Figs. 6 and 7. The solutions for symmetric buckling obtained by simultaneously solving Eqs. (29) and (67) for $\lambda_s \leq 38$ are also shown in Fig. 6. Comparisons with the FE results shows that Eq. (72) provides reasonable approximation for the symmetric buckling of fixed arches with the modified slenderness $\lambda_s \leq 38$ while Eq. (73) provides a lower bound approximation for the symmetric buckling of fixed arches with the modified slenderness $\lambda_s > 38$. The solutions for symmetric buckling obtained by simultaneously solving Eqs. (29) and (67) for $\lambda_s \leq 38$ agree well with the FE results.

In addition, the solution (64) is compared with the FE results for antisymmetric buckling in Fig. 6. This solution almost coincides with the FE results for shallow arches.

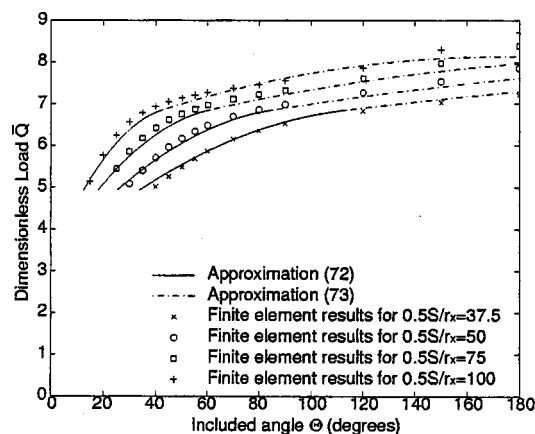


Fig. 7. Buckling of fixed arches against included angle

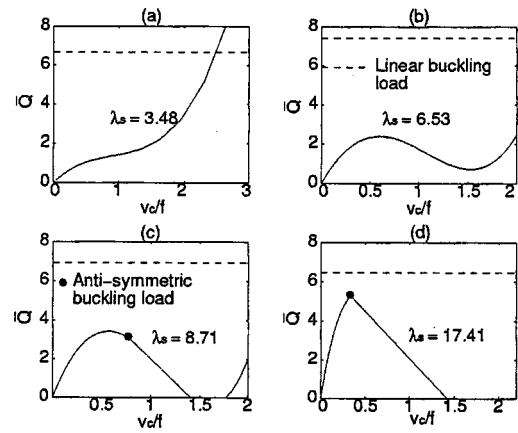


Fig. 8. Buckling and postbuckling behavior of pin-ended arches

Structural Behavior of Arches

Typical variations of the dimensionless load \bar{Q} with the dimensionless central vertical displacement v_c/f for pin-ended shallow arches are shown in Fig. 8, with Fig. 9 showing the counterparts for fixed shallow arches, where f is the arch rise. Four types of buckling and postbuckling behavior can be observed in Fig. 8, while three types of buckling and postbuckling behavior can be observed in Fig. 9. For the first type, there is no buckling as shown in Figs. 8(a) and 9(a). Pin-ended arches with a modified slenderness $\lambda_s \leq 3.91$ and fixed arches with $\lambda_s \leq 11.02$ are of this type. For the second type, the arches buckle in a symmetric mode without bifurcation as shown in Figs. 8(b) and 9(b). Pin-ended arches with a modified slenderness $3.91 \leq \lambda_s \leq 7.96$ and fixed arches with $11.02 \leq \lambda_s \leq 38.15$ are of this type. For the third type, the arches buckle in the symmetric snap-through mode first and then bifurcate antisymmetrically in the unstable region, i.e., on the descending branch of the load-deflection curve as shown in Figs. 8(c), and 9(c and d). Pin-ended arches with a modified slenderness $7.96 \leq \lambda_s \leq 9.80$ and fixed arches with $\lambda_s \geq 38.15$ are of this type. For the fourth type, the arches undergo antisymmetric bifurcation buckling, and the load carrying capacity of the arches decreases rapidly after this as shown in Fig. 8(d). Pin-ended shallow arches with a modified slenderness $\lambda_s \geq 9.80$ are of this type, but fixed shallow arches do not display this behavior as shown in Fig. 9(d). This indicates that the existence of antisymmetric bifurcation buckling loads is not a sufficient condition for antisymmet-

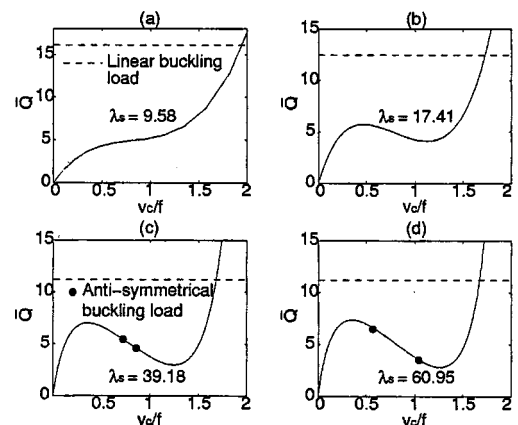


Fig. 9. Buckling and postbuckling behavior of fixed arches

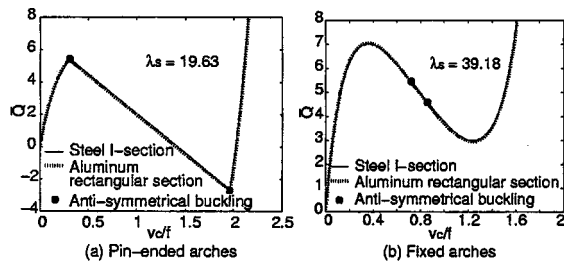


Fig. 10. Comparison of buckling and postbuckling behavior

ric bifurcation buckling to take place. The linear buckling loads predicted by the finite element program *PRFSA* (Papangelis et al. 1998) (that is based on classical buckling theory) are also shown in Figs. 8 and 9. It can be seen that the linear buckling loads are very unconservative. It can also be seen from Figs. 8 and 9 that the deflections are substantial when buckling occurs so that classical buckling theory, which does not consider the effects of pre-buckling deformations on buckling, cannot be used to predict the buckling load of shallow arches.

FE results for the buckling and postbuckling behavior of shallow arches with the same modified slenderness λ_s , but with different cross section and different material properties are shown in Fig. 10. Aluminum solid rectangular sections and steel I-sections were used for this study. The dimensions of these sections are identical with those considered previously, and the Young's modulus of elasticity was taken as $E=200,000$ MPa for steel and $E=80,150$ MPa for aluminum. It can be observed in Fig. 10 that the dimensionless load-deflection relationships between \bar{Q} and v_c/f for prebuckling, buckling, and postbuckling can be defined by the modified slenderness λ_s .

Concluding Remarks

The in-plane elastic stability of both pin-ended and fixed circular arches with a symmetric cross section subjected to a central concentrated load has been studied in this paper. Nonlinear equilibrium conditions for shallow arches have been established by the use of a virtual work formulation. Nonlinear buckling analysis provides accurate solutions for the symmetric and antisymmetric buckling of both pin-ended and fixed shallow arches. Approximate solutions have been proposed for the symmetric buckling load of pin-ended and fixed shallow arches. Comparisons with FE predictions have shown that the closed form solutions (47) for the antisymmetric buckling load of pin-ended shallow arches and the approximations (54) and (72) for the symmetric buckling load of pin-ended and fixed shallow arches are reasonably accurate. The approximation (59) provides good lower bound antisymmetric buckling loads for pin-ended nonshallow arches while Eq. (73) provides a reasonable approximation for symmetric buckling loads of fixed nonshallow arches. The symmetric mode governs the in-plane buckling of fixed arches under a central concentrated load. Existence of antisymmetric bifurcation buckling loads is not a sufficient condition for the antisymmetric buckling to take place.

A criterion for the classification of different types of fundamental buckling behavior has been established. The included

angle $\Theta = 90^\circ (\pi/2)$ can be used as the criterion for distinguishing between shallow and nonshallow pin-ended arches. For pin-ended nonshallow arches with the included angle $\Theta \geq 90^\circ (\pi/2)$, the buckling load can be predicted by the approximation (59). When $\Theta = 90^\circ (\pi/2)$, the solution (47) can be used to predict the buckling load of shallow arches whose modified slenderness $\lambda_s \geq 9.80$ while the approximation (54) can be used to predict the buckling load of arches with $3.91 \leq \lambda_s \leq 9.80$. For fixed arches with the modified slenderness $11.02 < \lambda_s \leq 38$, Eq. (72) can be used to approximate the symmetric buckling load while the approximation (73) can be used for the symmetric buckling load of fixed arches with $\lambda_s > 38$. Buckling does not occur for pin-ended arches with the modified slenderness $\lambda_s \leq 3.91$ or for fixed arches with the modified slenderness $\lambda_s \leq 11.02$.

Acknowledgment

This work has been supported by a research grant awarded to the first writer by the Australian Research Council under the ARC Large Research Grant Scheme.

Reference

- ABAQUS Standard User's Manual version 5.8. (1998). Hibbit, Karlsson and Sorensen Inc., Abaqus, Pawtucket, R.I.
- Bradford, M. A., Uy, B., and Pi, Y.-L. (2000). "In-plane stability of arches under a central concentrated load." *UNICIV Rep. No. 396*, the School of Civil and Environmental Engineering, Univ. of New South Wales, Sydney, Australia.
- Calhoun, P. R., and DaDeppo, D. A. (1983). "Nonlinear finite element analysis of clamped arches." *J. Struct. Eng.*, 109(3), 599–612.
- Column Research Committee of Japan, ed. (1971). *Handbook of structural stability*, Tokyo.
- Dickie, J. F., and Broughton, P. (1971). "Stability criteria for shallow arches." *J. Eng. Mech. Div.*, 97(EM3), 951–965.
- Elias, Z. M., and Chen, K. L. (1988). "Nonlinear shallow curved-beam finite element." *J. Eng. Mech.*, 114(6), 1076–1087.
- Galambas, T. V., ed. (1988). *Guide to stability design criteria for metal structures*, 4th Ed., Wiley, New York.
- Gjelsvik, A., and Bodner, S. R. (1962). "Energy criterion and snap-through buckling of arches." *J. Eng. Mech. Div.*, 88(EM5), 87–134.
- Johnston, B. G., ed. (1976). *Guide to stability design criteria for metal structures*, 3rd Ed., Wiley, New York.
- Kang, Y. J., and Yoo, C. H. (1994). "Thin-walled curved beams. II: Analytical solutions for buckling of arches." *J. Eng. Mech.*, 120(10), 2102–2125.
- Noor, A. K., and Peters, J. M. (1981). "Mixed model and reduced/selective integration displacement model for nonlinear analysis of curved beams." *Int. J. Numer. Methods Eng.*, 17(4), 615–631.
- Papangelis, J. P., Hancock, G. J., and Trahair, N. S. (1998). *PRFSA, version 3.0*. Centre for Advanced Structural Engineering, Univ. of Sydney, Sydney, Australia.
- Pi, Y.-L., and Bradford, M. A. (2002). "In-plane stability of arches." *Int. J. Solids Struct.*, 39(1), 105–125.
- Pi, Y.-L., and Trahair, N. S. (1998). "Non-linear buckling and postbuckling of elastic arches." *Eng. Struct.*, 20(7), 571–579.
- Rajasekaran, S., and Padmanabhan, S. (1989). "Equations of curved beams." *J. Eng. Mech.*, 115(5), 1094–1111.
- Schreyer, H. L., and Masur, E. F. (1966). "Buckling of shallow arches." *J. Eng. Mech. Div.*, 92(EM4), 1–17.
- Simitses, G. J. (1976). *An introduction to the elastic stability of structures*, Prentice-Hall, Englewood Cliffs, N.J.

- Stolarski, H., and Belytschko, T. (1982). "Membrane locking and reduced integration for curved elements." *ASME Trans. J. Appl. Mech.*, 49(1), 172–176.
- Timoshenko, S., and Gere, J. M. (1961). *Theory of elastic stability*, McGraw-Hill, New York.
- Trahair, N. S., and Bradford, M. A. (1998). *The behavior and design of steel structures to AS4100*, 3rd Ed., Australian, E&FN Spon, London.
- Vlasov, V. Z. (1961). *Thin-walled elastic beams*, 2nd Ed., Israel Program for Scientific Translation, Jerusalem, Israel.
- Wen, R. K., and Suhendro, B. (1991). "Nonlinear curved-beam element for arch structures." *J. Struct. Eng.*, 117(11), 3496–3515.